THE JOURNAL OF BIOLOGICAL CHEMISTRY VOL. 284, NO. 18, pp. 12136–12144, May 1, 2009
© 2009 by The American Society for Biochemistry and Molecular Biology, Inc. Printed in the U.S.A.

Covalently Bound Substrate at the Regulatory Site of Yeast Pyruvate Decarboxylases Triggers Allosteric Enzyme Activation[S]

Received for publication, August 12, 2008, and in revised form, February 17, 2009 Published, JBC Papers in Press, February 26, 2009, DOI 10.1074/jbc.M806228200

Steffen Kutter[‡], Manfred S. Weiss[§], Georg Wille[‡1], Ralph Golbik[‡], Michael Spinka[‡], and Stephan König[‡2]

From the [‡]Institute for Biochemistry and Biotechnology, Faculty of Biological Sciences, Martin-Luther-University Halle-Wittenberg, Kurt-Mothes-Str. 3, 06120 Halle (Saale) and the [§]European Molecular Biology Laboratory Outstation, c/o Deutsches Elektronen Synchrotron (DESY), Notkestr. 85, 22603 Hamburg, Germany

The mechanism by which the enzyme pyruvate decarboxylase from two yeast species is activated allosterically has been elucidated. A total of seven three-dimensional structures of the enzyme, of enzyme variants, or of enzyme complexes from two yeast species, three of them reported here for the first time, provide detailed atomic resolution snapshots along the activation coordinate. The prime event is the covalent binding of the substrate pyruvate to the side chain of cysteine 221, thus forming a thiohemiketal. This reaction causes the shift of a neighboring amino acid, which eventually leads to the rigidification of two otherwise flexible loops, one of which provides two histidine residues necessary to complete the enzymatically competent active site architecture. The structural data are complemented and supported by kinetic investigations and binding studies, providing a consistent picture of the structural changes occurring upon enzyme activation.

Pyruvate decarboxylases (EC 4.1.1.1) catalyze the non-oxidative decarboxylation of pyruvate, yielding acetaldehyde and carbon dioxide. Together with the enzyme alcohol dehydrogenase (EC 1.1.1.1), which reduces the acetaldehyde to ethanol with the help of the co-substrate NADH, it represents the metabolic pathway of alcoholic fermentation. PDC[3] is localized in the cytosol of cells from yeasts, plant seeds, and a few bacteria. The catalytic activity of PDC depends on the presence of the cofactor thiamine diphosphate (ThDP), which is bound mainly via a divalent metal ion (magnesium in most cases) to the protein moiety. Many detailed kinetic studies have been published on yeast PDC wild types (1–9). A number of *Sc*PDC variants were analyzed, too (1–9). Some active site variants (E51A, D28A, E477Q) proved to be almost catalytically inactive. PDCs are multisubunit enzymes. The typical molecular mass of one subunit is 59–61 kDa. The tetramer is the catalytically active state of most PDCs. Higher oligomers (octamers) have been described for PDCs from plant seeds (10, 11) or some fungi (12). However, studies on structure function relationships of yeast PDCs showed that the dimer is the minimum functional unit of the enzyme displaying considerable catalytic activity (13, 14). The two closely related pyruvate decarboxylases from *Saccharomyces cerevisiae* (*Sc*PDC) and *Kluyveromyces lactis* (*Kl*PDC) are well characterized ThDP-dependent enzymes, which share 86.3% identical amino acid residues. They have been studied in great detail by means of kinetic investigations and spectroscopic studies. Both enzymes are allosterically regulated as reflected by sigmoid steady state kinetics and lag phases in their progress curves. The substrate PYR activates the initially inactive yeast PDCs in a time-dependent manner. Kinetic studies reveal a slow isomerization as triggered by substrate binding to a separate regulatory site (15). A number of substrate surrogates have been identified, which are able to activate PDC as well. The effects of pyruvamide (PA; for the chemical structure, see Scheme 1) on the activation kinetics have been studied in detail for *Sc*PDC (15) and for *Kl*PDC (16). Phosphonate analogues (among them methyl acetylphosphonate, MAP, Scheme 1) of pyruvate have been applied to elucidate the catalytic cycle (17–21) or to trap reaction intermediates in crystal structures (22–24). Chemical modification of PDCs with group-specific reagents pointed to an important role of cysteine residues (25). Site-directed mutagenesis of cysteine residues to alanine or serine demonstrated that residue Cys-221 might be the decisive one for enzyme activation (1, 4, 26, 27). Consequently, it was postulated that the region around Cys-221 is the regulatory site of PDC, and formation of a thiohemiketal at this side chain was proposed. However, a number of questions remained elusive. (i) How is the activator fixed at the regulatory site? (ii) What are the prime structural properties of the active state as compared with the inactive state? (iii) How is the signal transmitted from the regulatory to the active site? (iv) Which are the decisive features of the active site in the activated state that render efficient catalysis possible? To answer these questions, we present here the crystal structures of *Kl*PDC with the bound substrate surrogate MAP and of the *Sc*PDC variants D28E and E477Q with bound substrate PYR along with kinetic

The atomic coordinates and structure factors (codes 2VJY, 2VK1 and 2VK8) have been deposited in the Protein Data Bank, Research Collaboratory for Structural Bioinformatics, Rutgers University, New Brunswick, NJ (http://www.rcsb.org/).

[S] The on-line version of this article (available at http://www.jbc.org) contains two supplemental tables and two supplemental figures.

[1] Present address: Institute for Biophysics, Dept. of Physics, Johann-Wolfgang-Goethe-University Frankfurt/Main, Max-von-Laue-Str. 1, 60438 Frankfurt/Main, Germany.

[2] To whom correspondence should be addressed. Tel.: 49-345-5524829; Fax: 49-345-5527014; E-mail: stephan.koenig@biochemtech.uni-halle.de.

[3] The abbreviations used are: PDC, pyruvate decarboxylase; *Sc*PDC, pyruvate decarboxylases from *Saccharomyces cerevisiae*; *Kl*PDC, pyruvate decarboxylases from *Kluyveromyces lactis*; ThDP, thiamine diphosphate; MAP, methyl acetylphosphonate; PYR, pyruvate; PA, pyruvamide; SAXS, small angle x-ray solution scattering; PEG, polyethylenglycol; MES, 4-morpholineethanesulfonic acid; r.m.s.d., root mean square deviation.

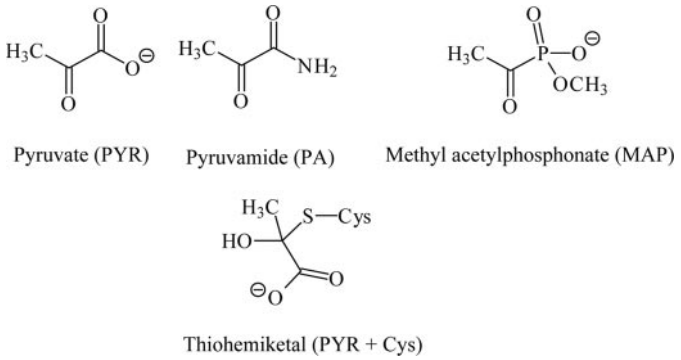

SCHEME 1. **Chemical structures of the substrate pyruvate, the activators pyruvamide and methyl acetylphosphonate, and the thiohemiketal from pyruvate and cysteine, respectively.**

studies on the activating effect of both activators and binding studies using the small angle x-ray solution scattering (SAXS) method.

EXPERIMENTAL PROCEDURES

Enzyme Purification—The recombinant wild type and the variants D28A and E477Q have been purified according to the procedures of Killenberg-Jabs *et al.* (3), *Kl*PDC according to Kutter *et al.* (28).

Protein Crystallization—*Kl*PDC was dissolved in 20 mM citrate buffer, pH 6.1, 1 mM dithiothreitol, 5 mM ThDP, 5 mM $MgSO_4$, 80 mM MAP. The same solution without MAP, but with 7–23% (w/v) PEG 2000/PEG 6000 (1:1 ratio) as precipitant, was used as reservoir. Well diffracting crystals were obtained after 10 days equilibration at 8 °C at 20% PEG and 1 mg of *Kl*PDC per ml. Stored stock solutions of *Sc*PDC variants were diluted into 12 mM citrate/1.3 mM MES, pH 6.3, 1.3 mM dithiothreitol, 1.3 mM ThDP, 1.3 mM $MgSO_4$, 630 mM PYR, 5 μg of yeast alcohol dehydrogenase per ml, 2 mM $NADH+H^+$. A buffer containing 18 mM citrate/2 mM MES, pH 6.3, 2 mM dithiothreitol, 2 mM ThDP, 2 mM $MgSO_4$ together with 7–24% (w/v) PEG 2000/PEG 6000 (1:1 ratio) was used as reservoir solution. Well diffracting crystals resulted from these batches after 14 days of incubation on ice at PEG concentration of 22.5% (w/v) and 1 mg of enzyme per ml.

Data Collection, Structure Determination, and Refinement—For cryoprotection, crystals were incubated in a 1:1 mixture of reservoir and an aqueous solution of 32–42% (w/v) PEG 400 and 5% (v/v) glycerol for 1 min (in the case of MAP-*Kl*PDC, 10–15 s). Diffraction data were collected at the beamlines X12 (European Molecular Biology Laboratory (EMBL) Outstation Hamburg c/o DESY) and ID14-2 (European Synchrotron Radiation Facility (ESRF), Grenoble, France). For indexing, integration, and scaling, the programs Denzo and Scalepack (29) were used. Intensities were converted to structure factor amplitudes using the program Truncate (30). *Kl*PDC (PDB ID code 2VK4) was used as a search model for the MAP-*Kl*PDC complex, and PA-*Sc*PDC (PDB ID code 1QPB) was

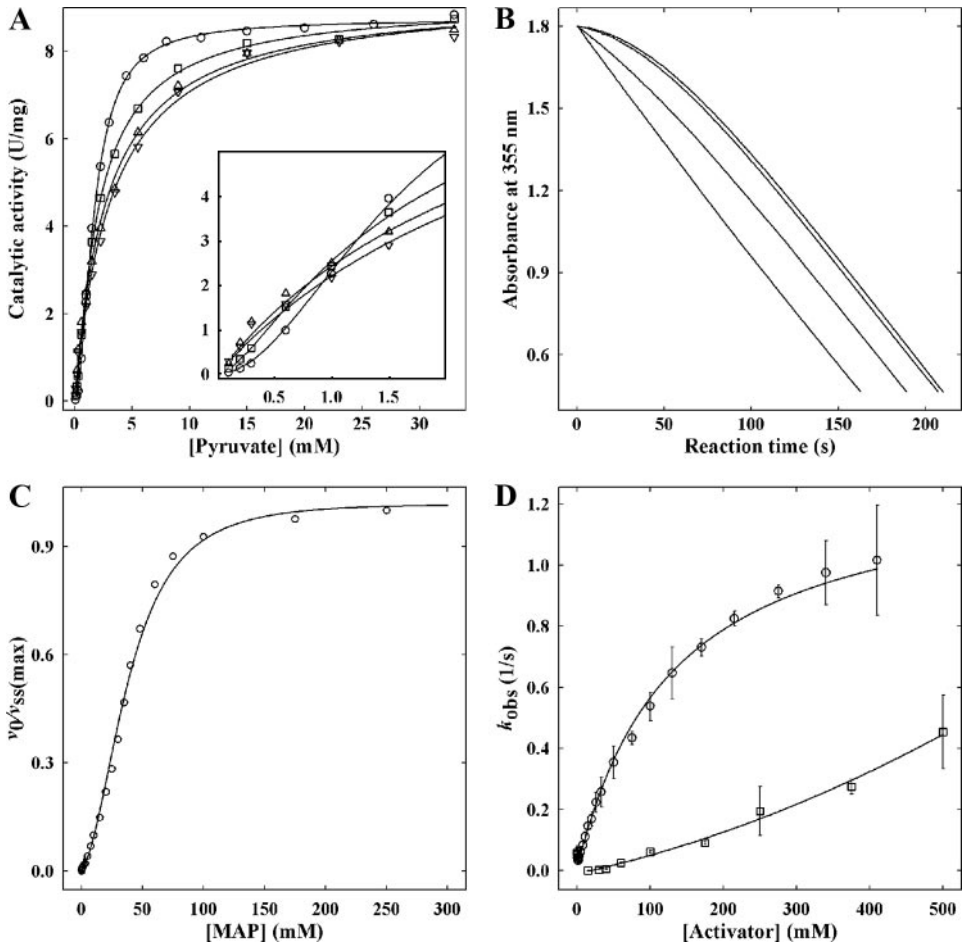

FIGURE 1. **MAP kinetics.** *A*, influence of MAP on the shape of the *v versus* [*S*] plot (*circles*, 0 mM MAP, *squares*, 20 mM MAP, *triangles*, 40 mM MAP, and *inverse triangles*, 75 mM MAP). The *lines* represent sigmoid fits according to equation $v([S]) = V_{max} \cdot [S]^2/(A + B \cdot [S] + [S]^2)$ with the following values for the parameters for V_{max} (units/mg), *A* (mM^2), and *B* (mM), respectively, 0 mM MAP, 8.77, 2.52, 0.27; 20 mM MAP, 9.16, 0.72, 1.88; 40 mM MAP, 9.30, 10^{-9}, 2.83; 75 mM MAP, 9.39, 10^{-9}, 3.26. The uncertainties of these values are less than 20% throughout, except for the *A* values in the presence of 40–75 mM MAP, which are essentially zero, demonstrating Michaelis-Menten behavior of the activated enzyme with *B* as apparent K_m. *Inset*, enlarged view at low substrate concentrations. *B*, transients of the *Kl*PDC-catalyzed reaction at 3 mM PYR after preincubation with MAP (increasing concentrations from top to bottom as in *A*). For better comparison, original data are normalized to the steady state rate and to the same initial absorbance. *C*, dependence of the ratio of initial rate (v_0) and steady state rate (v_{SS}) on MAP concentration. The rates were obtained from transients (see *B* for primary data) according to Equation 2. The *line* represents a fit to the equation $v_0/v_{SS} = K_1 [L] + [L]^2/(A + K_1 \cdot [L] + [L]^2)$ with $A = K_L \cdot K_{ilo} \cdot K_1$. The dissociation constants correspond to Scheme 2, and [*L*] represents the MAP concentration during preincubation. Fit parameters are $K_1 = 2.5 \pm 2$ mM, $A = 1460 \pm 142$ mM^2. *D*, activator concentration dependence of the apparent activation rate constant k_{obs} (*circles*, PYR; *squares*, MAP). The k_{obs} values were obtained from discontinuous measurements (for details, see the section "Kinetic Measurements"). The *error bars* represent the fitting errors. In the absence of MAP, the *line* represents the fit according to the equation $k_{obs} = k_{iso} \cdot [S]/([S] + K_a) + k_{-iso} \cdot K_{mS}/(K_{mS} + [S])$ (16); in the presence of MAP, a line is drawn for better visualization only.

used as a search model for the PYR-*Sc*PDC$_{D28A}$ complex and for the PYR-*Sc*PDC$_{E477Q}$ complex. Refinement was realized with the program Refmac5 (30).

Determination of Protein Concentration—Whenever possible, the protein concentration was determined spectrophotometrically from the UV-spectra at 280 nm (Jasco V-560 UV/VIS spectrophotometer) using a molar extinction coefficient of 60,000 $M^{-1}\cdot cm^{-1}$ for one PDC subunit. In all other cases, the Bradford method (31) was applied.

Kinetic Measurements—All measurements were carried out at 10 °C and pH 6.0, the optimum of catalytic activity, according to the coupled optical assay of Holzer *et al.* (32). In this assay, acetaldehyde, the product of the PDC-catalyzed reaction, is reduced with NADH to ethanol by the auxiliary enzyme alcohol dehydrogenase. A protein concentration of 120 μg/ml yeast alcohol dehydrogenase (catalytic activity 300 units/mg) guarantees the suppression of artifactual lag phases. 0.05 M MES buffer, pH 6.0, 0.15 M ammonium sulfate and an observation wavelength of 355 nm were applied. The corresponding extinction coefficient for NADH at this wavelength was determined to be 4764 $M^{-1}\cdot cm^{-1}$. Preincubation experiments using MAP have been carried out in two different manners. First, PDC (1 mg/ml) was incubated for 30 min in the presence of varying MAP concentrations. The test reaction was started by a 1:500 dilution of the preincubation mixture into the test assay. Subsequently, full progress curves were recorded to determine the initial (v_0) and the steady state velocity (v_{SS}). In this case, the MAP concentrations in the preincubation mixture and the assay mixture were identical.

Secondly, the enzyme (6.7 mg/ml) was incubated with several MAP concentrations (15–500 mM) at 25 °C in a time-dependent manner. For each MAP concentration, a series of measurements were taken after different preincubation times *t*. To determine $v_0(t)$ after each individual preincubation run, an aliquot from the preincubation mix was diluted (1:500) into the test assay. The Holzer assay was carried out at 10 °C. In this type of experiment, the test did not contain any MAP except the amount introduced by the aliquot taken from the preincubation mixture. The empirical $v_0(t)$ values were fitted according to

$$v_0(t) = v_{final}(1 - e^{-k_{obs}t}) \qquad \text{(Eq. 1)}$$

SAXS with Synchrotron Radiation—Measurements were performed at beamline X33 at the EMBL Hamburg outstation c/o DESY (camera length 2.7 m, MAR345 image plate detector, vacuum sample cell) at 16 °C and at protein concentrations of ~2.5 mg/ml. The buffer system was the same as used for kinetic measurements, but 2 mM dithiothreitol was added. The momentum transfer axis s ($s = 4\pi\sin\theta/\lambda$, where 2θ is the scattering angle, and $\lambda = 0.15$ nm, the x-ray wavelength) was calibrated using collagen or tripalmitin as standards. The scattering patterns were collected for 120 s. MAR image files were extracted during data collection for intensity normalization (transmitted flux, detector response, scaling of the *s* axis) by the data reduction program Automar (33). Buffer scattering was subtracted using the program Primus-mar (34). The molecular masses were obtained from the ratio of the forward scattering intensity $I_{(0)}$ of the samples and that of the molecular mass standard bovine serum albumin.

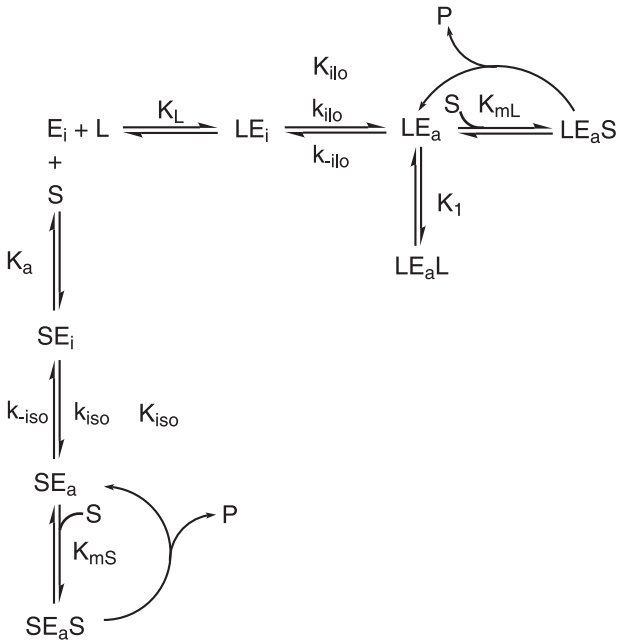

SCHEME 2. **Proposed kinetic model for the allosteric activation of yeast pyruvate decarboxylases in simultaneous presence of both the substrate *S* and the artificial activator *L*.** K_a and K_L are the primary dissociation constants at the regulatory site for *S* and *L*, respectively. k_{iso} and k_{ilo} represent the forward rate constants for the conformation change driven by *S* and *L*, respectively. k_{-iso} and k_{-ilo} are the associated rate constants for the reverse reaction. K_{iso} and K_{ilo} are defined by $K_{iso} = (k_{-iso}/k_{iso})$ and $K_{ilo} = (k_{-ilo}/k_{ilo})$, respectively. K_{mS} is the Michaelis-Menten constant for the substrate-activated enzyme, whereas K_{mL} refers to the ligand-activated enzyme. K_1 is the dissociation constant of the artificial activator for the ligand-activated enzyme. Ligands/substrates written on the *left* of the enzyme species are bound to the regulatory site of the enzyme, and those written on the *right* are bound to the active site. In the absence of *L*, this activation scheme reduces to the established model of reference (16).

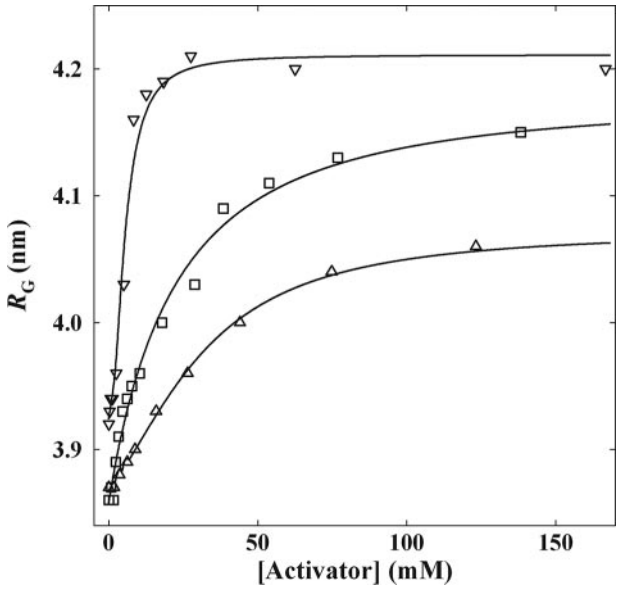

FIGURE 2. **Dependence of the scattering parameter R_G of PDC on the concentration of the added activator.** In the case of PA and MAP, *Kl*PDC was used, and in the case of PYR, *Sc*PDC$_{E477Q}$ was used (*triangles*, PA; *squares*, MAP; *inverse triangles*, PYR; *lines*, hyperbolic fits for *Kl*PDC, sigmoid fit for *Sc*PDC$_{E477Q}$). The following values for half-saturation were obtained: for PYR, 5.7 ± 0.23 mM ($n = 1.85$); for MAP, 20.7 ± 2.39 mM; for PA, 37.8 ± 1.36 mM).

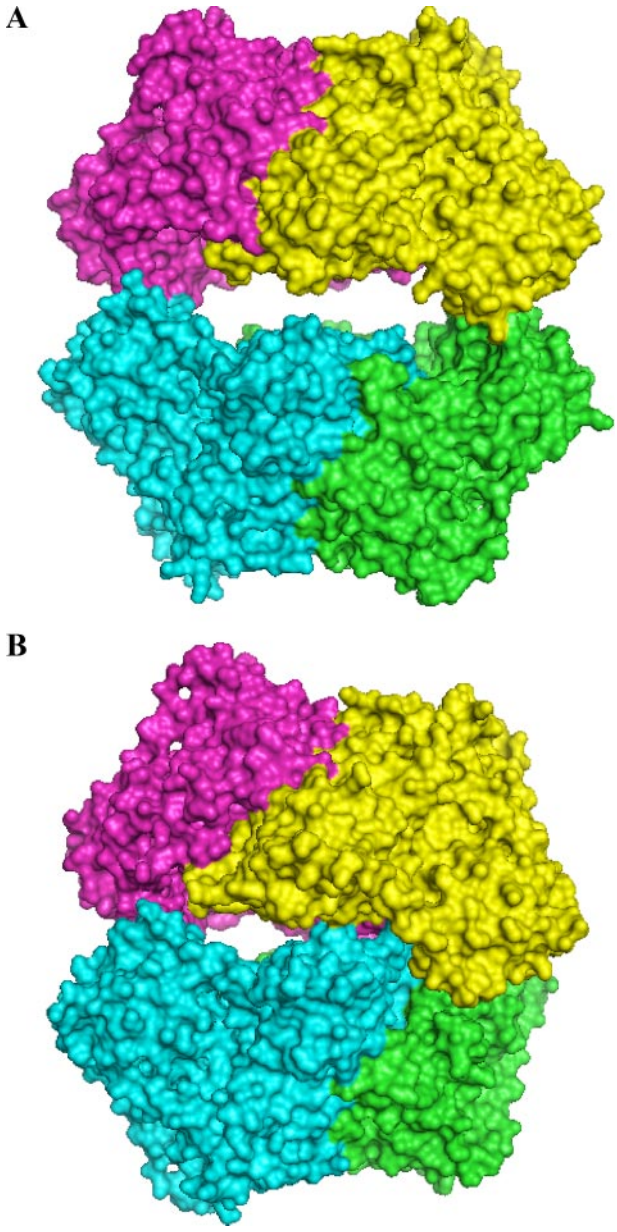

FIGURE 3. **The overall crystal structures of PDC tetramers representing MAP-*Kl*PDC and PYR-*Sc*PDC variants in *A* and of native *Kl*PDC (28), PA-*Sc*PDC (38), and ketomalonate-activated ScPDC (39) in *B*.** The subunits are shown with different colors in *space-filling mode*.

TABLE 1

Data collection and refinement statistics for MAP-*Kl*PDC, PYR-*Sc*PDC$_{D28A}$, and PYR-*Sc*PDC$_{E477Q}$

Parameter	MAP-*Kl*PDC	PYR-*Sc*PDC$_{D28A}$	PYR-*Sc*PDC$_{E477Q}$
pdb ID	2VJY	2VK1	2VK8
Beamline	X12	ID14-2	ID14-2
Detector	MARCCD	ADSC Q4R CCD	ADSC Q4R CCD
Wavelength (Å)	0.93001	0.933	0.933
Temperature (K)	100	100	100
Crystal detector distance (mm)	220	125	101
Rotation range per image (°)	0.5	0.5	0.5
Total number of images	437	360	360
Resolution range (Å)	104.26-2.30	99.0-1.71	95.4-1.42
(Highest resolution shell)	(2.34-2.30)	(1.74-1.71)	(1.44-1.42)
Space group	$P2_1$	$P2_1$	$P2_1$
Unit cell parameters (Å, °)	a=81.76, b=135.77, c=107.26, β=103.88	a=80.88, b=141.31, c=114.41, β=107.19	a=78.98, b=190.51, c=84.14, β=113.01
Mosaicity (°)	0.79	0.38	0.40
Total number of reflections	438,157	937,903	1,523,231
Unique reflections	100,426	262,151	427,276
Redundancy	4.4	3.6	4.4
I/σ(I)	9.6 (2.3)	17.5 (2.1)	22.5 (1.9)
Completeness (%)	99.7 (99.9)	99.3 (99.2)	99.7 (99.8)
R_{merge} (%)	14.8 (61.5)	6.8 (57.4)	5.3 (62.9)
$R_{r.i.m.}$ (%)	16.8 (70.6)	8.0 (68.0)	n.d.
$R_{p.i.m.}$ (%)	8.0 (34.3)	4.2 (36.1)	n.d.
Overall B-factor (Wilson plot, Å^2)	29.7	20.8	17.6

Parameter	MAP-*Kl*PDC	PYR-*Sc*PDC$_{D28A}$	PYR-*Sc*PDC$_{E477Q}$
Total number of used reflections	99345	260330	425935
Total number of atoms (non-hydrogen)	18588	18994	19242
Number of protein atoms	17344	17280	17292
Number of water molecules	1048	1558	1818
R_{cryst} (%)	15.4 (19.2)	19.1 (24.8)	18.1 (25.4)
R_{free} (%)	22.5 (30.5)	22.0 (27.6)	18.6 (26.7)
Total number of reflections for R_{free}	1006	1313	1068
Bond length (r.m.s.d. from ideality, Å)	0.025	0.018	0.013
Bond angles (r.m.s.d. from ideality, °)	1.95	1.45	1.25
Ramachandran plot (% in most favoured regions)	89.5	90.9	91.3
Ramachandran plot (% in allowed regions)	99.8	100	100
Average B-factor (Å^2)	26.3	20.9	18.9

$$R_{r.i.m.} = \frac{100 \cdot \sum_{hkl} \sqrt{\frac{N}{N-1}} \cdot \sum_i (I_i(hkl) - I(hkl))}{\sum_{hkl} \sum_i I_i(hkl)}, \quad R_{p.i.m.} = \frac{100 \cdot \sum_{hkl} \sqrt{\frac{1}{N-1}} \cdot \sum_i (I_i(hkl) - I(hkl))}{\sum_{hkl} \sum_i I_i(hkl)},$$

where $I_i(hkl)$ is the intensity of the observation i of the reflection hkl and N is the redundancy (41).

RESULTS AND DISCUSSION

Kinetic Effects of MAP

As MAP was used as a substrate surrogate in crystallographic studies on *Kl*PDC, it was of paramount importance to demonstrate that this analogue does indeed act as an activator of this enzyme. In the absence of any effectors, *Kl*PDC displays typical sigmoidal steady state kinetics (16). After incubation of the enzyme with MAP, the sigmoidicity of the *v versus* [*S*] plot becomes gradually suppressed with increasing analogue concentrations (Fig. 1*A*). At a MAP concentration of 75 mM, the steady state kinetics of the enzyme is essentially hyperbolic. Moreover, at PYR concentrations below 1 mM, the activating effect of MAP is also documented by the higher absolute values of the steady state rates v_{SS} (Fig. 1*A*, *inset*). This effect is even more apparent from the corresponding progress curves (Fig. 1*B*). In the absence of MAP, the progress curves of *Kl*PDC show lag phases, which reflect the conversion of the initial inactive enzyme state into the activated enzyme state (16) according to the substrate-driven branch in Scheme 2. Empirical progress curves can be fitted to Equation 2, which conforms to the mechanism in Scheme 2 (16, 35).

$$A = A_0 - v_{ss} \cdot t + \frac{v_{ss} - v_0}{k_{obs}} \cdot [1 - \exp(-k_{obs} \cdot t)] \quad \text{(Eq. 2)}$$

with A, absorbance at time t, A_0, initial absorbance, k_{obs}, the observed first order rate constant for the substrate activation process, v_0, the initial velocity, and v_{SS}, the steady state velocity. Upon preincubation of *Kl*PDC with MAP, the initial reaction rate (v_0) is increased as the concentration of potentially active enzyme (LE_a, LE_aL in Scheme 2) generated by the activator analogue increases. Eventually, at a MAP concentration of 75 mM, the progress curve appears to be a straight line in accordance with the hyperbolic *v versus* [*S*] plots obtained under the very same conditions (Fig. 1, *A* and *B*). Initial rates (v_0) and steady state rates (v_{SS}) can be evaluated from empirical progress curves (Equation 2, for details, see Krieger *et al.* (16)). The plot of the ratio v_0/v_{SS} *versus* MAP concentration (Fig. 1*C*) clearly demonstrates that MAP is able to completely activate *Kl*PDC.

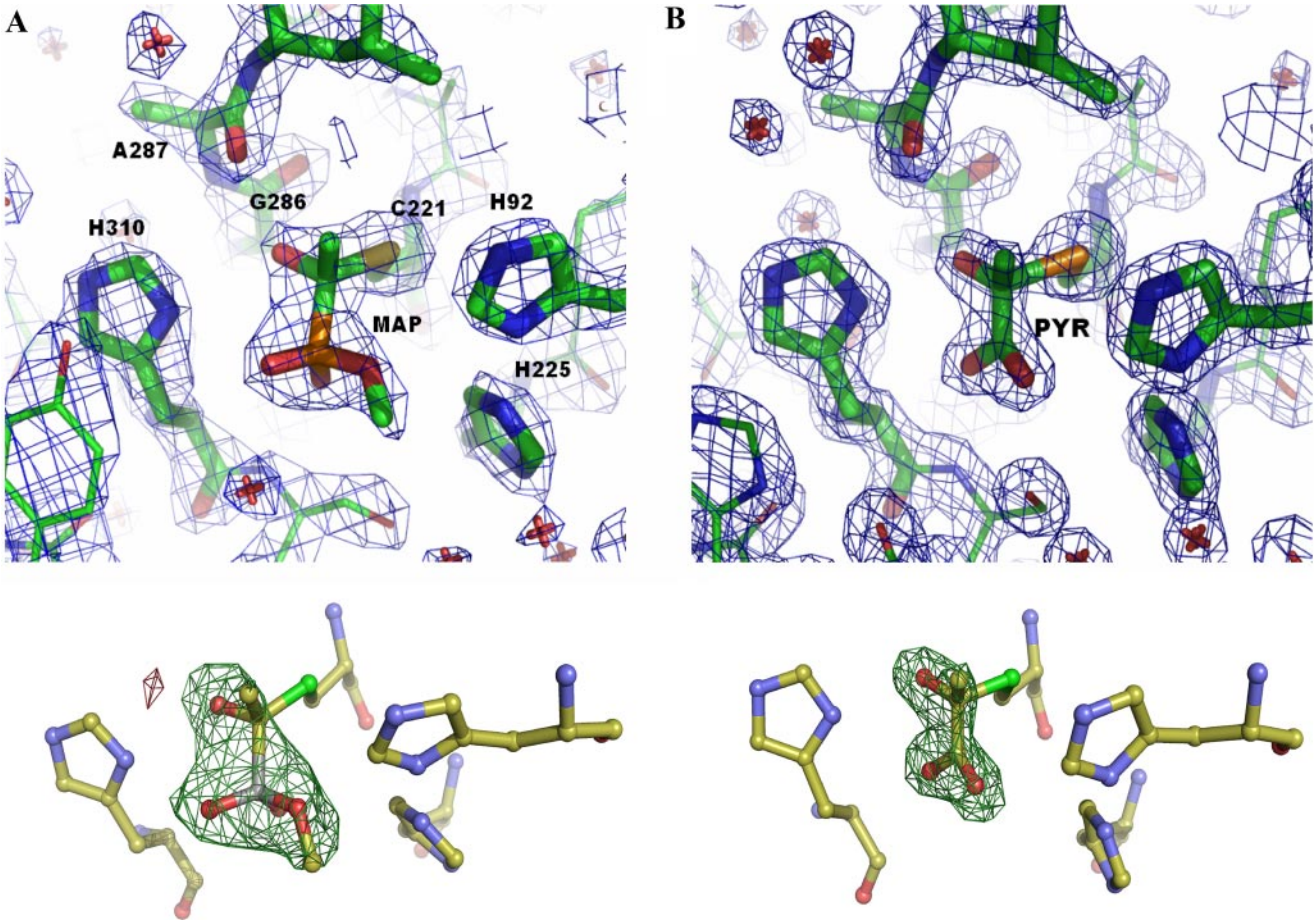

FIGURE 4. **View of the regulatory sites with the activators bound covalently to residue Cys-221 for MAP-*Kl*PDC (*A*) and PYR-*Sc*PDC$_{E477Q}$ (*B*).** Electron density is shown at a σ-level of 2.0 in the $2F_o - F_c$ map (*blue*) and at a σ-level of 4.0 in the omit map (*green*). Amino acid residues are illustrated in *stick mode*. The labeled residues can directly interact with the thiohemiketal. Labels in *A* correspond also to *B*.

For MAP, an effective half-saturation value of 35 mM can be extracted from the sigmoidal fit in Fig. 1*C*. Time-dependent preincubation studies revealed that the MAP-triggered activation of *Kl*PDC is a rather slow process as compared with the activation by its native substrate PYR (Fig. 1*D*). Taking the chemical structures of both compounds into account (Scheme 1), the additional methyl residue and the bulky phosphonate moiety of MAP, as compared with the carboxylate of PYR, may cause a steric hindrance for the binding at the enzyme molecule. In the presence of MAP substrate, saturation is reached at slightly higher substrate concentrations (Fig. 1*A*), pointing to a weak competitive inhibition by this effector. In summary, the kinetic data presented here demonstrate that MAP is an activator for yeast PDCs, thus justifying its application in crystallographic studies. The preliminary kinetic model in Scheme 2 essentially illustrates the competition of substrate and activator molecules for the regulatory site in accordance to the crystallographic findings detailed below. Binding of either substrate or activating ligands at the regulatory site triggers a slow transition of the initially inactive enzyme form into the activated one. The rate-limiting step of this transition is the protein isomerization associated with the rate constants k_{iso} and k_{ilo}, respectively. All other steps are assumed to be fast by comparison. In terms of the model, the dependence of k_{obs} on the concentration of PYR in Fig. 1*D* relates to the substrate-driven branch, whereas the dependence of k_{obs} on the concentration of MAP is reflected in the ligand-driven branch. Additionally, the mechanism allows for the competition effects for the active site in the activated state being present in the steady state data.

Activator Binding Studies Using SAXS

It had been demonstrated earlier (36) that addition of PA to *Sc*PDC resulted in a significant increase of the radius of gyration R_G, the scattering parameter describing the maximum distance of two points within a particle in solution. These changes in R_G had been interpreted in terms of a global rearrangement within the protein molecule without alteration of the oligomerization state of the enzyme (because of the unchanged forward scattering intensity $I_{(0)}$, which correlates with the molecular mass of the particle). Here we illustrate, to the best of our knowledge for the first time, the activator concentration dependence of R_G for the binding of PA and MAP to *Kl*PDC and of the substrate PYR to the catalytically inactive variant *Sc*PDC$_{E477Q}$. All plots exhibit a clear saturation of the ligand binding (Fig. 2). The increase of the R_G values in the presence of the ligands reflects the formation of activated enzyme species (LE_a and LE_aL). As shown in Fig. 2, MAP and PA have similar half-saturation values for *Kl*PDC (21 and 38 mM, respectively) and for *Sc*PDC (27 and 35 mM, respectively, data not shown).

However, by far the lowest half-saturation value is found for the native substrate PYR with a value of 5.7 mM. This finding corresponds to the striking difference between K_a and K_L (Scheme 2) as illustrated in Fig. 1*D*. The increase of R_G, in turn, is similar for MAP and PYR binding (0.31 and 0.29 nm). The lowest shift of R_G was found with PA (0.21 nm). Notably, the half-saturation values of MAP drawn from spectroscopic activation kinetics and SAXS binding studies, respectively, conform closely to each other (36 mM from Fig. 1*C* and 21 mM from Fig. 2). This indicates that both methods monitor the same process.

So far, only two types of overall tetramer crystal structures of yeast PDCs are known, the open (37) and half-side closed (28, 38, 39) conformation (Fig. 3). The described increase of R_G by activator binding can be interpreted as a conformation change from the half-side closed to the open tetramer form. Moreover, theoretical scattering patterns can be calculated from both crystal structure models by using the program Crysol (40). On this basis, volume fractions of the corresponding tetramer forms can be calculated from the experimental scattering patterns (34) for all the applied activator concentrations. Surprisingly, the resulting plot is superimposable to the plot of R_G *versus* activator concentration illustrated in Fig. 2.

Structural Implications

Overall Structures—The crystal structure of *Kl*PDC in complex with MAP was determined to 2.3 Å resolution, and those of the *Sc*PDC variants in complex with PYR were determined to 1.7 Å (D28A) and 1.4 Å resolution (E477Q), respectively (for details, see Table 1). The final models comprise four times 562 amino acid residues, each of the subunits harboring one cofactor molecule ThDP, one Mg^{2+}, and two molecules of activator. The asymmetric units contain the PDC tetramer. The overall folds of the subunits within one dimer (Fig. 3) are almost identical to that of native species (*Kl*PDC, r.m.s.d. 2.28 Å for 1116 superimposed Cα-atoms, *Sc*PDC$_{E477Q}$, r.m.s.d. 0.97 Å for 1074 superimposed Cα-atoms, *Sc*PDC$_{D28A}$, r.m.s.d. 0.96 Å for 1074 superimposed Cα-atoms). Differences were found at the surface of the tetramer, *i.e.* at the middle domains and the C-terminal α-helices. The MAP molecules are located at the active sites of *Kl*PDC with distances of 2.22 Å between the Cα-atoms of MAP and the C2 atoms of ThDP within one tetramer and at the regulatory sites, covalently bound to Cys-221 (bond length 1.82 Å). PYR molecules are found with distances of 1.69 Å (Cα–C2) at the active sites and 2.12 Å (Cα–S) at the regulatory sites in *Sc*PDC$_{D28A}$ and with distances of 2.04 Å to Cys-221 of *Sc*PDC$_{E477Q}$ but not in the active sites of the latter variant. The absence of PYR in the active site of *Sc*PDC$_{E477Q}$ might be associated with the disrupted thiazolium ring of the cofactor molecule in this species. The tetramers of MAP-*Kl*PDC, PYR-*Sc*PDC$_{D28A}$, and PYR-*Sc*PDC$_{E477Q}$ are superimposable without significant differences (r.m.s.d. of 0.5–0.6 Å for 2248 Cα-atoms) All three crystal structures represent the open and planar tetramer conformation (Fig. 3*A*), which is fixed by the rigidification of the middle domain together with two loop regions (104–113 and 288–304).

Loop Structuring—The most salient feature common to all activated structures described herein is the well defined elec-

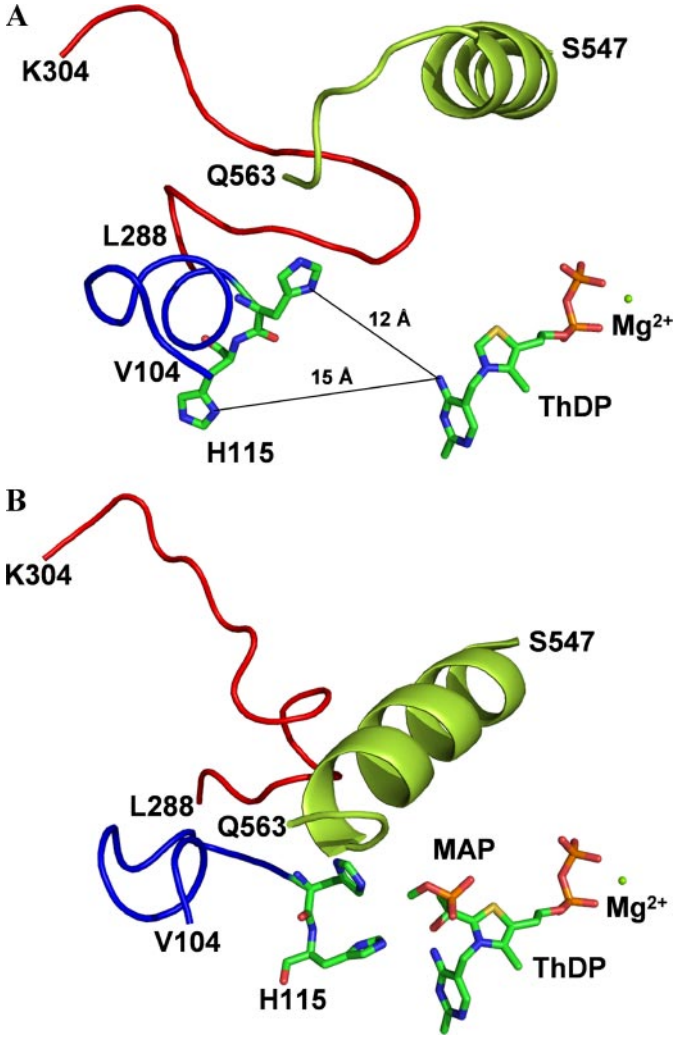

FIGURE 5. **View from the surface of *Kl*PDC molecule down to one active site.** *A* and *B*, the location of the histidine residues 114 and 115 in native *Kl*PDC (*A*)- and MAP-activated *Kl*PDC (*B*). The cofactor ThDP and the histidine residues are presented in *stick mode* (individually colored atoms), and all other residues are shown as a tube of the Cα line, with loop 104–113 in *blue*, loop 288–304 in *red*, and the C-terminal helix in *green*.

tron density for two loop regions (residues 104–113 and 288–304, respectively), which is virtually absent in the crystal structure of native *Sc*PDC (37) or poorly defined in the structure of native *Kl*PDC (28). It may therefore be concluded that loop structuring and loop translocation are the decisive events in the activation process. The gained rigidity of both loop regions at all subunits within the tetramer enforces the planar and symmetric dimer arrangement within the tetramer (Fig. 3*A*). Both loops are located in the neighborhood of the active site at the core region of the tetramer (see Figs. 5 and 6). It should be noted that these loops, although cooperating in the completion of one active site, belong to different subunits (38). In the frozen state, these loop regions are stabilized internally by a number of H-bonds (see Fig. 6*C* and supplemental materials). Loop 104–113 additionally develops a short α-helix and closes partially over the active site. His-114 and His-115, the next upstream neighbors of loop 104–113, are part of the active site. For His-114, an essential function in PDC catalysis has been proposed from kinetic studies with accordant variants from yeast and

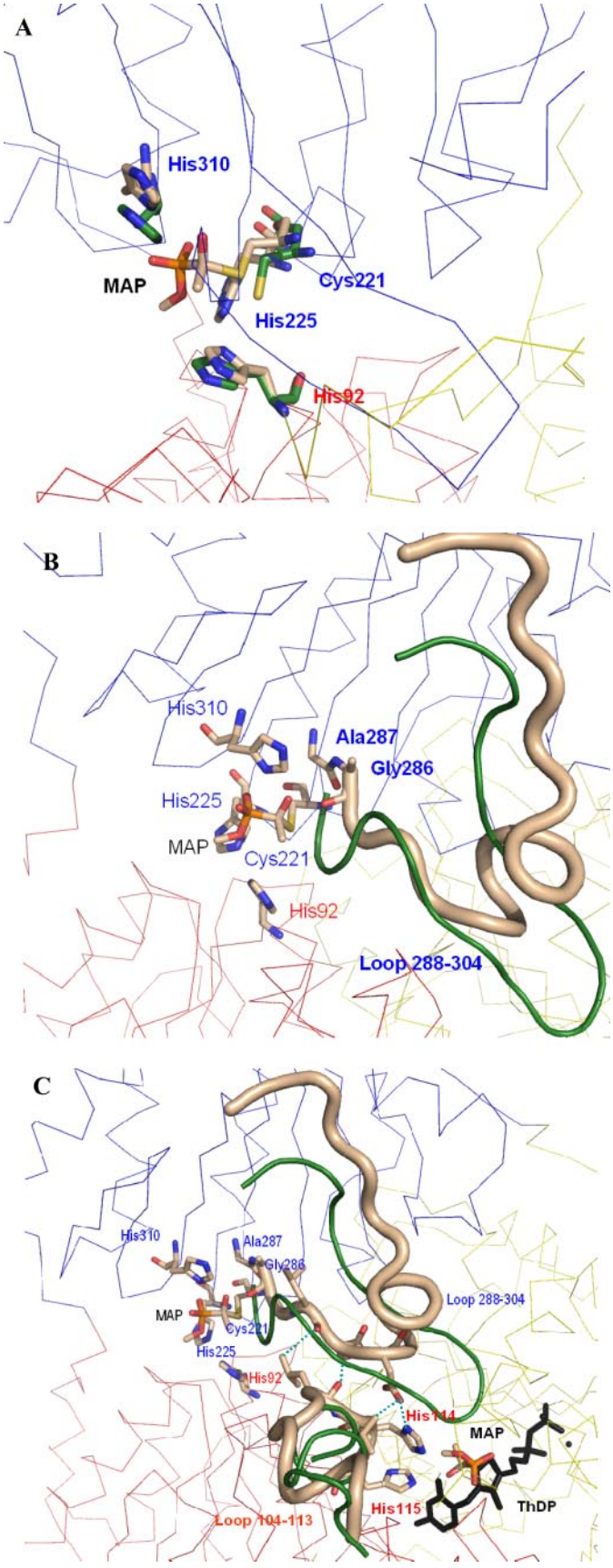

FIGURE 6. **Snapshots of the signal transduction pathway from the regulatory to the active site in yeast PDCs.** The different subunits are shown as Cα trace in different colors, the labeled residues are shown as *sticks*, and the color of the label is that of the subunit the residue belongs to. *A*, overlay of one regulatory site before (carbon atoms in *green*) and after covalent binding of the activator MAP at Cys-221 (carbon atoms in *beige*). The 4 Å shift of the thiohemiketal is clearly to be seen. *B*, the shift of the thiohemiketal causes direct interactions to residues Ala-286 and Gly-287 and restructures the whole loop region 288–304 (*beige tube*; loop conformation before activation is shown in *green*). *C*, the structured loop 288–304 induces direct interactions to the other loop region 104–113, and the H-bonds between both loops are illustrated as *blue dashed lines*. The new conformation of this loop (*beige*, loop conformation before activation in *green*) reorients the adjacent residues His-114 and His-115, which now can directly interact with the activator molecule bound at the C2 atom of ThDP.

bacteria (7, 8, 42, 43). Tittmann *et al.* (44) postulated a specific role for His-114 (together with Asp-28) during release of the reaction product acetaldehyde. Because of the location of both loop regions in the tetramer core, *i.e.* the inner interface between two dimers of the tetramer, crystal contacts can clearly be excluded as reason for loop structuring.

Regulatory Site—The most striking result of this study is the evidence for a covalent C–S bond at the side chain of Cys-221 in the activated structures, confirming results of studies on the activation mechanism by chemical modification (25) and mutation of cysteine residues (1, 4, 26, 27) in *Sc*PDC. The covalent character of this bond is well documented by the crystallographic C–S distance (1.82 Å) as well as by the tetrahedral configuration at the former carbonyl carbon of both MAP (Fig. 4*A*) and PYR (Fig. 4*B*). Notably, the sp^3 character of the Cα-atom of PYR in both activated *Sc*PDC variants is somewhat less developed than that of the equivalent carbon atom in the MAP-activated *Kl*PDC. Together with the longer distances between the Cα-atom of PYR and the S-atom of Cys-221, this could be indicative of a dynamic equilibrium of non-covalently and covalently bound PYR at the regulatory site. Apart from Cys-221, the following residues are located in vicinity (within a 5 Å distance) to the bound activator (for MAP-*Kl*PDC): His-92, Arg-161, His-225, Gly-286, Ala-287, Leu-288, His-310, Ser-311, Tyr-313, Met-326, and five waters. Thus, the regulatory site is predominantly lined by positively charged side chains, which can interact electrostatically with the phosphonate moiety of MAP or the carboxylate moiety of PYR, respectively. This electrostatic interaction might guide the negatively charged activator molecule to the regulatory site. Surprisingly, H-bonds are only formed from main chain carbonyl oxygen atoms of Gly-286 and Ala-287 to the α-hydroxyl group (the former carbonyl group) of the covalently bound MAP.

Effects on the Active Site—Interestingly, all side chains constituting the active site apart from Asp-28, His-114, and His-115 remain unaffected by the binding of the activators at Cys-221. Furthermore, no significant distortion of the vital V-conformation of the cofactor is seen in the activated state. However, a comparison of the native and the MAP-activated crystal structures of *Kl*PDC revealed that the two amino acids His-114 and His-115 undergo marked structural reorientations upon activator binding (Fig. 5). The histidine side chains are now directed toward the substrate-binding site, *i.e.* the distances of their ring nitrogens to the C2 atom of the cofactor ThDP are diminished from 12–15 to 6–7 Å. Concomitantly, the main chain of residue Asp-28/Ala-28 is rotated by ~35°, and the side chain is orientated toward His-115. This reorien-

tation basically restructures the active site into its enzymatically competent architecture, triggered by activator binding at Cys-221. A survey of all Cα-atom shifts recorded upon activation is given in the supplemental information.

Signal Transfer from the Thiohemiketal at Cys-221 to the Active Site—The question of how the signal of activation is transmitted from Cys-221 to the active site is a matter of debate that has not been decided to this very day. What can be drawn about signal transduction from the new structures? Firstly, the formation of the thiohemiketal at Cys-221, which itself is not part of either loop, shifts the side chain of this amino acid about 4 Å from its original position in the native structures (Fig. 6*A*). Subsequently, this conformation change enforces the reorientation of a number of amino acid residues in the interaction radius of the thiohemiketal, such as His-92, His-225, Gly-286, Ala-287, His-310, and Ser-311 (Fig. 6*B*). The arising interaction network fixes the complete R-domain. Loop 288–304 is part of that domain and is completely restructured. This loop forms a number of interactions with another, originally flexible loop 104–113 of the PYR domain of the adjacent subunit, especially residues Leu-289, Ser-290, and Asp-291, with residues Leu-112, Leu-113 and becomes structured itself (Fig. 6*C*). Due to this interaction between both loops, the signal is transmitted to the other subunit within the functional dimer. Further stabilization of the loop 104–113 arises from interactions with the C-terminal helix, which in the activated state closes over the active site (Fig. 5*B*). The position of the latter is now identical to those in the three-dimensional structures of the non-activated species *Zm*PDC (pyruvate decarboxylase from *Zymomonas mobilis*) (45) and *Ec*IPDC (indolepyruvate decarboxylase from *Enterobacter cloacae*) (46). Eventually, the signal is transmitted to His-114 and His-115, which adopt a new orientation (Figs. 5*B* and 6*C*). These conformation changes in the vicinity of the cofactor ThDP make the active site now competent for effective catalysis and binding of the substrate.

Molecular Causes of Cofactor Activation—Phenomenologically, the activation of *Sc*PDC and *Kl*PDC is reflected in lag phases of their respective progress curves as well as in the sigmoidal shape of the steady state kinetics (15, 16). Both enzyme species are potentially inactive at the start of the reaction (15, 16, 47). A decade ago, Kern *et al.* (48) have shown that the prime molecular target of activation in *Sc*PDC is the deprotonation at the C2 atom of ThDP, which requires a tremendous shift of the pK_a value of the C2 proton to become catalytically competent (49). The structural basis of this kinetic effect remained, however, largely elusive. Evidently, some structural differences between the active sites in the native and the activated state must account for the observed acceleration of the H/D exchange at the C2 atom of the cofactor as triggered by activation in both yeast PDCs. The results of the current crystallographic study allow some preliminary insight. First and foremost, the active site as such is complete only in the activated state. A vital role has been ascribed to His-113 in *Zm*PDC, as part of a catalytic dyad supporting aldehyde release (44, 50). Its position is equivalent to that of His-114 in *Sc*PDC and *Kl*PDC, respectively, which reorients upon activation. Both histidines, His-114 and His-115, are required for efficient catalysis. Moreover, the H114F/H115F variant, although being almost inactive, shows perfect Michaelis-Menten behavior, pointing to abolished activation (7). These observations alone, however, do not yet explain the accelerated deprotonation at the C2 atom of the cofactor, as neither His-114 nor His-115 is specifically involved in this process. Secondly, the structured loops, particularly the region 104–113, shield the active site against the solvent. Thus, the microenvironment of the cofactor is probably less polar in the activated than in the native state. A non-polar environment dramatically promotes deprotonation at the C2 atom of the cofactor as the neutral ylide species is generated in this process (51). Thus, the partial closure of the active site might well be the decisive molecular cause of the activation of the cofactor. Thirdly, solvent shielding might likewise contribute to the stabilization of non-polar reaction intermediates, as *e.g.* the enamine and, additionally, promote the general sequestration of substrates and intermediates. On the other hand, substrate molecules must have access to the active site during catalysis. Therefore, the active site cannot be totally shielded from the solvent. It should be noted that even the rigidified loop structures retain a considerable measure of mobility, which allows substrate access. It remains to be clarified whether a quasi-periodic closure and reopening of the active site in the activated state is coupled to particular stages of the catalytic cycle as advocated by Kluger and Smyth (52) or is even synchronized with a dynamic alternation between covalently and non-covalently associated PYR at Cys-221 as proposed by Alvarez *et al.* (53) and defended recently by Schowen (54). Finally, the question arises as to why nature chose thiohemiketal formation, a rare mode of covalent modification, which is, to the best of our knowledge, unique as a principle of enzyme regulation. Probably, thiohemiketal formation was favored as PYR lacks an extended hydrophobic moiety that could function as a partner in non-covalent ligand-protein interaction.

Acknowledgments—We thank the Jordan group at Rutgers for the variants D28A and E477Q, Birgitta Seliger for preparation of the enzyme species from S. cerevisiae, and Anja Seidel and Robert Eckensthaler for crystallization of MAP-KlPDC. Access to EMBL beamlines X12 and X33 at the DORIS storage ring, DESY, Hamburg and to beamline ID14-2 at the ESRF in Grenoble is acknowledged.

REFERENCES

1. Baburina, I., Gao, Y., Hu, Z., Jordan, F., Hohmann, S., and Furey, W. (1994) *Biochemistry* **33,** 5630–5635
2. Killenberg-Jabs, M., König, S., Hohmann, S., and Hübner, G. (1996) *Biol. Chem. Hoppe-Seyler* **377,** 313–317
3. Killenberg-Jabs, M., König, S., Eberhardt, I., Hohmann, S., and Hübner, G. (1997) *Biochemistry* **36,** 1900–1905
4. Baburina, I., Li, H., Bennion, B., Furey, W., and Jordan, F. (1998) *Biochemistry* **37,** 1235–1244
5. Li, H., Furey, W., and Jordan, F. (1999) *Biochemistry* **38,** 9992–10003
6. Li, H., and Jordan, F. (1999) *Biochemistry* **38,** 10004–10012
7. Liu, M., Sergienko, E. A., Guo, F. S., Wang, J., Tittmann, K., Hübner, G., Furey, W., and Jordan, F. (2001) *Biochemistry* **40,** 7355–7368
8. Sergienko, E. A., and Jordan, F. (2001) *Biochemistry* **40,** 7369–7381
9. Joseph, E., Wei, W., Tittmann, K., and Jordan, F. (2006) *Biochemistry* **45,** 13517–13527
10. Mücke, U., König, S., and Hübner, G. (1995) *Biol. Chem. Hoppe-Seyler* **376,** 111–117
11. Zehender, H., Trescher, D., and Ullrich, J. (1987) *Eur. J. Biochem.* **167,** 149–154
12. Alvarez, M. E., Rosa, A. L., Temporini, E. D., Wolstenholme, A., Panzetta, G., Patrito, L., and Maccioni, H. J. F. (1993) *Gene* (*Amst.*) **130,** 253–258
13. Killenberg-Jabs, M., Jabs, A., Lilie, H., Golbik, R., and Hübner, G. (2001)

Eur. J. Biochem. **268,** 1698–1704
14. Kutter, S., Spinka, M., Koch, M. H. J., and König, S. (2007) *Prot. J.* **26,** 585–591
15. Hübner, G., Weidhase, R., and Schellenberger, A. (1978) *Eur. J. Biochem.* **92,** 175–181
16. Krieger, F., Spinka, M., Golbik, R., Hübner, G., and König, S. (2002) *Eur. J. Biochem.* **269,** 3256–3263
17. Biryukov, A. I., Bunik, V. I., Zhukov, Y. N., Khurs, E. N., and Khomutov, R. M. (1996) *FEBS Lett.* **382,** 167–170
18. Bunik, V. I., Biryukov, A. I., and Zhukov, Y. N. (1992) *FEBS Lett.* **303,** 197–201
19. Kluger, R., and Nakaoka, K. (1974) *Biochemistry* **13,** 910–914
20. Kluger, R., and Pike, D. C. (1977) *J. Am. Chem. Soc.* **99,** 4504–4506
21. O'Brien, T. A., Kluger, R., Pike, D. C., and Gennis, R. B. (1980) *Biochim. Biophys. Acta* **613,** 10–17
22. Arjunan, P., Sax, M., Brunskill, A., Chandrasekhar, K., Nemeria, N., Zhang, S., Jordan, F., and Furey, W. (2006) *J. Biol. Chem.* **281,** 15296–15303
23. Bera, A. K., Polovnikova, L. S., Roestamadji, J., Widlanski, T. S., Kenyon, G. L., McLeish, M. J., and Hasson, M. S. (2007) *J. Am. Chem. Soc.* **129,** 4120–4121
24. Wille, G., Meyer, D., Steinmetz, A., Hinze, E., Golbik, R., and Tittmann, K. (2006) *Nat. Chem. Biol.* **2,** 324–328
25. Hübner, G., König, S., and Schellenberger, A. (1988) *Biomed. Biochim. Acta* **47,** 9–18
26. Zeng, X. P., Farrenkopf, B., Hohmann, S., Dyda, F., Furey, W., and Jordan, F. (1993) *Biochemistry* **32,** 2704–2709
27. Wang, J., Golbik, R., Seliger, B., Spinka, M., Tittmann, K., Hübner, G., and Jordan, F. (2001) *Biochemistry* **40,** 1755–1763
28. Kutter, S., Wille, G., Relle, S., Weiss, M. S., Hübner, G., and König, S. (2006) *FEBS. J.* **273,** 4199–4209
29. Otwinowski, Z., and Minor, W. (1997) *Methods Enzymol.* **276,** 307–326
30. Collaborative Computational Project Number 4 (1994) *Acta Crystallogr. Sect. D Biol. Crystallogr.* **50,** 760–763
31. Bradford, M. (1976) *Anal. Biochem.* **72,** 248–254
32. Holzer, H., Schultz, G., Villar-Palasi, C., and Jüntgen-Sell, J. (1956) *Biochem. Z.* **327,** 331–344
33. Petoukhov, M. V., Konarev, P. V., Kikhney, A. G., and Svergun, D. I. (2007) *J. Appl. Crystallogr.* **40,** 223–228
34. Konarev, P. V., Volkov, V. V., Sokolova, A. V., Koch, M. H. J., and Svergun, D. I. (2003) *J. Appl. Crystallogr.* **36,** 1277–1282
35. Werther, T., Spinka, M., Tittmann, K., Schütz, A., Golbik, R., Mrestani-Klaus, C., Hübner, G., and König, S. (2008) *J. Biol. Chem.* **283,** 5344–5354
36. Hübner, G., König, S., Schellenberger, A., and Koch, M. H. J. (1990) *FEBS Lett.* **266,** 17–20
37. Arjunan, P., Umland, T., Dyda, F., Swaminathan, S., Furey, W., Sax, M., Farrenkopf, B., Gao, Y., Zhang, D., and Jordan, F. (1996) *J. Mol. Biol.* **256,** 590–600
38. Lu, G., Dobritzsch, D., Baumann, S., Schneider, G., and König, S. (2000) *Eur. J. Biochem.* **267,** 861–868
39. Furey, W., Arjunan, P., Chen, L., Sax, M., Guo, F., and Jordan, F. (1998) *Biochim. Biophys. Acta* **1385,** 253–270
40. Svergun, D., Barberato, C., and Koch, M. H. J. (1995) *J. Appl. Cryst.* **28,** 768–773
41. Weiss, M. S. (2001) *J. Appl. Cryst.* **34,** 130–135
42. Candy, J. M., Koga, J., Nixon, P. F., and Duggleby, R. G. (1996) *Biochem. J.* **315,** 745–751
43. Huang, C. Y., Chang, A. K., Nixon, P. F., and Duggleby, R. G. (2001) *Eur. J. Biochem.* **268,** 3558–3565
44. Tittmann, K., Golbik, R., Uhlemann, K., Khailova, L., Schneider, G., Patel, M., Jordan, F., Chipman, D. M., Duggleby, R. G., and Hübner, G. (2003) *Biochemistry* **42,** 7885–7891
45. Dobritzsch, D., König, S., Schneider, G., and Lu, G. (1998) *J. Biol. Chem.* **273,** 20196–20204
46. Schütz, A., Sandalova, T., Ricagno, S., Hübner, G., König, S., and Schneider, G. (2003) *Eur. J. Biochem.* **270,** 2312–2321
47. Hübner, G., and Schellenberger, A. (1986) *Biochem. Int.* **13,** 767–772
48. Kern, D., Kern, G., Neef, H., Tittmann, K., Killenberg-Jabs, M., Wikner, C., Schneider, G., and Hübner, G. (1997) *Science* **275,** 67–70
49. Washabaugh, M. W., and Jencks, W. P. (1988) *Biochemistry* **27,** 5044–5053
50. Schenk, G., Leeper, F. J., England, P., and Duggleby, R. G. (1997) *Eur. J. Biochem.* **248,** 63–71
51. Crosby, J., and Lienhard, G. E. (1970) *J. Am. Chem. Soc.* **92,** 5707–5716
52. Kluger, R., and Smyth, T. (1981) *J. Am. Chem. Soc.* **103,** 1214–1216
53. Alvarez, F. J., Ermer, J., Hübner, G., Schellenberger, A., and Schowen, R. L. (1995) *J. Am. Chem. Soc.* **117,** 1678–1683
54. Schowen, R. L. (2007) *Isot. Environ. Health Stud.* **43,** 1–16